EXPERIMENT K-6-09

MORPHOLOGICAL AND BIOCHEMICAL INVESTIGATION OF MICROGRAVITY-INDUCED NERVE AND MUSCLE BREAKDOWN

PART I: INVESTIGATION OF NERVE AND MUSCLE BREAKDOWN DURING SPACEFLIGHT

PART II: BIOCHEMICAL ANALYSIS OF EDL AND PLT MUSCLES

Principal Investigator:

D.A. Riley
Department of Anatomy and Cellular Biology
Medical College of Wisconsin
Milwaukee, Wisconsin 53225

Co-Investigators:

S. Ellis
San Jose State University
San Jose, California

J. Bain, F. Sedlak, G. Slocum
Medical College of Wisconsin
Milwaukee, Wisconsin 53225

V. Oganov
Institute of Biomedical Problems
Moscow, USSR

EXPERIMENT K-6-09

PART I: INVESTIGATION OF NERVE AND MUSCLE BREAKDOWN DURING SPACEFLIGHT

D.A. Riley, J. Bain, F. Sedlak, and G. Slocum

SUMMARY

The present findings on rat hindlimb muscles suggest that skeletal muscle weakness induced by prolonged spaceflight can result from a combination of muscle fiber atrophy, muscle fiber segmental necrosis, degeneration of motor nerve terminals and destruction of microcirculatory vessels. Damage was confined to the red adductor longus (AL) and soleus muscles. The midbelly region of the AL muscle had more segmental necrosis and edema than the ends. Macrophages and neutrophils were the major mononucleated cells infiltrating and phagocytosing the cellular debris. Toluidine blue-positive mast cells were significantly decreased in Flight AL muscles compared to controls; this indicated that degranulation of mast cells contributed to tissue edema. Increased ubiquitination of disrupted myofibrils may have promoted myofilament degradation. Overall, mitochondria content and SDH activity were normal, except for a decrease in the subsarcolemmal region. The myofibrillar ATPase activity shifted toward the fast type in the Flight AL muscles. Some of the pathological changes may have occurred or been exacerbated during the 2 day postflight period of readaptation to terrestrial gravity. While simple atrophy should be reversible by exercise, restoration of pathological changes depends upon complex processes of regeneration by stem cells. Initial signs of muscle and nerve fiber regeneration were detected. Even though regeneration proceeds on Earth, the space environment may inhibit repair and cause progressive irreversible deterioration during long term missions. Muscles obtained from Flight rats sacrificed immediately (within a few hours) after landing are needed to distinguish inflight changes from postflight readaptation.

INTRODUCTION

Extended exposure of humans to microgravity produces progressive skeletal muscle weakness. The mechanism of the loss of strength must be understood in order to develop rational countermeasures. Our previous flight investigation of rats flown 1 week aboard Spacelab 3 (SL3) revealed that most of the soleus (Sol) muscle fibers exhibited simple atrophy, but up to 1% of the fibers showed segmental necrosis (Riley et al., 1987). Muscle atrophy and necrosis as well as evidence for degeneration of blood vessels and motor nerve terminals were observed previously for 3 week Cosmos Biosatellite missions (Gazenko et al., 1978; Baranski et al., 1979; Ilyina-Kakueva & Portugalov, 1981; Ilyin, 1983; Takacs et al., 1983). Disruption of motor innervation appears to occur after 1 week because neuromuscular junctions appeared normal in the SL3 Flight animals. In the present study, the sol, adductor longus (AL), plantaris (Plt), and extensor digitorum longus (EDL) muscles were examined from rats orbited 12.5 days in Cosmos 1887. These specimens allowed us to determine quantitatively that both muscle atrophy and necrosis were progressive. Furthermore, degeneration of microcirculatory vessels and motor nerve terminals were detected.

METHODS

Preparation of tissues. Selected muscles were obtained immediately following decapitation of rats from the Basal, Vivarium, Flight, and Synchronous groups. The caudal (posterior) one third of the AL and the distal third of the EDL muscles were removed by cutting with a fine scissors. Each

piece was separately pinned on a stretch on a flat stick. The specimens were fixed in vials for 2 to 12 hours at 20±2 deg C in 4% glutaraldehyde, 2% paraformaldehyde, buffered at pH 7.4 with 0.1 M cacodylate containing 5 mM $CaCl_2$. The vials were transferred to a refrigerator at 2 to 10 deg C for 24 or 50 hours until rinsed in the calcium containing buffer at room temperature for 3 hours. After rinsing, the specimens were removed from the sticks and postfixed for 2 to 2.5 hours in 1.3% osmium tetraoxide in the calcium- containing cacodylate buffer. The postfixed specimens were rinsed and stored in 0.1 M cacodylate buffer at 2 to 10 deg C for 3 to 6 weeks before routine dehydration in ethanols, clearing in propylene oxide and infiltration in epoxy resin. Half of each muscle was en bloc stained with uranyl acetate before initiating dehydration. Following resin polymerization at 60 and 90 deg C, semithin (0.5 μm) and ultrathin sections were cut for light and electron microscopic examination. Ultrathin sections were poststained with uranyl acetate and lead citrate before examination in a JEOL 100 CXII electron microscope.

Plt muscles and the remaining portions of the AL and EDL muscles were put individually on labeled index cards and quick frozen by immersing in liquid nitrogen. Frozen muscles were stored in liquid nitrogen until shipped at -70 deg C to the Medical College of Wisconsin. Upon arrival, portions of the frozen EDL and Plt muscles were removed by transecting with a cold razor blade to obtain specimens for assays of tripeptidyl aminopeptidase II, calcium activated protease, carbonic anhydrase III and parvalbumin by Dr. Ellis in San Jose State, California. These portions were repackaged and shipped on dry ice. The remaining specimens were stored in liquid nitrogen until frozen sectioned (10 μm) with a cryostat microtome at -25 deg C.

Tissue section staining. Serial sections were collected on glass slides and stained as follows: hematoxylin and eosin, toluidine blue, and histochemical enzyme activities of alkaline and acid myofibrillar ATPase, NADH and succinic dehydrogenase activities, alpha glycerophosphate dehydrogenase, and acid phosphatase as well as immunohistochemical localization of ubiquitin conjugates and tripeptidyl aminopeptidase (Riley & Allin, 1973; Riley et al., 1987; Haas, 1988; Riley et al., 1988a). Sections of Flight and Synchronous Sol muscles were kindly provided by Dr. Edgerton for H&E staining for assessment of atrophy and aberrant fiber content; this permitted comparison of changes in the Sol muscles of Cosmos 1887 and Spacelab 3.

Light microscopic quantitation. The percentages of aberrant fibers were determined in the H&E sections of AL, EDL, Plt and Sol muscles; aberrant fibers consisted of mononuclear cell-invaded fibers with segmental necrosis and small angular fibers with central nuclei.

Fast twitch glycolytic (FG), fast twitch glycolytic oxidative (FOG), and slow twitch oxidative (SO) were classified using the histochemical staining properties as defined previously (Riley et al., 1987). Alkaline ATPase reacted sections of AL muscles were utilized for areal measurements of SO and FOG fibers in all groups. At least 100 fibers of each type were traced on paper at a final magnification of X98.5 using a Tri Simplex projector. Fiber areas were determined by computerized planimetry of the traced images (Bioquant II). Similar areal measurements were performed on the SO, FOG, and FG fibers of the EDL and Plt muscles.

Mast cells were counted in sections of Flight and Synchronous AL muscles stained with toluidine blue. The number of cells was normalized per section, per section unit area, and per muscle fiber number.

Electron microscopic quantitation Z line length and mitochondrial content. The AL muscles of Flight rats nos. 7 and 9 showed much higher levels of fiber necrosis than Flight rats nos. 6, 8 and 10. Since it was difficult to assess atrophic changes in myofibrils and mitochondria of severely disrupted fibers, ultrastructural quantitation was performed in rats 6, 8 and 10. Two micrographs each of 7 fibers, chosen at random, were printed at 30,000 magnification. All of the Z lines totally within the micrograph were measured by the length paradigm on a computerized digitizing pad. The mean length was determined for each rat, and a grand mean was calculated for each group and

compared statistically. The concentrations of mitochondria in the subsarcolemmal region (3 μm depth), within A band and non-A band regions of the myofibrils in cross sections were determined for 10 fibers/rat by areal digitizing planimetry as described previously (Riley et al., 1987).

RESULTS

Muscle fiber type changes. In the alkaline myofibrillar ATPase reacted sections of AL muscles, the SO fibers were lightly stained, the FOG fibers were darkly stained and the intermediate fibers were moderately reactive (Figs. 1,2). The average number of intermediate fibers per section was 233±47 for Flight muscles which was significantly greater ($p<0.003$) than the number (19±17) in comparable Synchronous control sections. Since there was no difference in the average number of dark fibers in the muscles of the Flight and Synchronous groups (213±44 and 206±35, respectively) the intermediate fibers represented transformation of the lightly staining fibers to moderately staining fibers.

The percentages of fiber types was determined for the Flight and Synchronous AL, EDL, and Plt muscles (Table 1). The Flight AL muscles showed an 18% increase in intermediate fibers and a concomitant decrease in SO fibers. No changes in fiber type percentages occurred in the Flight EDL and Plt muscles.

Muscle fiber atrophy. Overall, the mean cross sectional area of Flight AL fibers was 36% less than that of the Synchronous control (Figs. 1-4). When assessed at the fiber type level, the average area of SO fibers in the ATPase sections of Flight AL muscles was significantly ($p<0.001$) less (43.8%) than that of the Synchronous controls (Table 2). The approximately 16% atrophy of the intermediate and FOG fibers in Flight AL muscles was not significantly different from values for comparable fiber types in the Synchronous controls (Table 2).

On the basis of the myofibrillar ATPase reaction three fiber types were defined in the EDL and Plt muscles. SO fibers were light, FOG fibers were dark, and FG fibers were moderate (Riley et al., 1982). The mean areas of all three fiber types were decreased in both muscles (Table 2). For the Plt, the decrease was significant for all fiber types; in the EDL, only the atrophy of the FOG fibers was significant.

Occurrence of aberrant muscle fibers. Two types of aberrant fibers were observed at the light microscopic level: small angular fibers with central nuclei (Fig. 3) and fibers exhibiting segmental necrosis with partial or total invasion by mononucleated cells (Figs. 2,4,5,6). Pronounced interstitial edema was present in the AL and Sol Flight muscles, but not in the EDL and Plt Flight muscles (Figs. 5,6). Flight AL muscles contained both types of aberrant fibers with segmental necrosis accounting for more than 80% of the aberrant fiber population. The Synchronous, Vivarium, and Basal control muscles possessed only the small angular type of aberrant fibers; this was also true for both the EDL and Plt muscles. The mean percentage of aberrant fibers was significantly increased in the Flight AL muscles compared to the control values (Table 3). There were no significant differences in aberrant fiber content between the control groups (Table 3).

The Flight Sol (n=3) exhibited significantly ($p<.001$) more (6.8±0.8%) necrotic fibers compared to only 0.9±0.1% in the Synchronous control (Fig. 6). As in the AL, greater than 80% of the damaged fibers in the Flight Sol were undergoing segmental necrosis. No necrotic fibers were present in the EDL and Plt Flight muscles. Aberrant fibers in these muscles were all angular fibers with central nuclei, and no differences in the mean percentages of aberrant fibers per muscle section was observed for either the EDL Flight (.07±.03%) and Synchronous (.07±.02%) muscles (n=3 rats) or the Plt Flight (.12±.02%) and Synchronous (.08±.02%) muscles (n=3 rats).

Toluidine blue-stained mast cells were counted in sections of Flight and Synchronous AL muscles. In both groups, degranulation was rare. The vast majority of cells were densely packed with blue

granules (Fig. 7). Flight ALs had fewer mast cells/section (4.5±1.3) than that of Synchronous muscles which contained 8.8±1.1 cells/section ($p<.05$, 1 tailed t-test). When the number of mast cells was normalized to muscle fiber number, the Flight muscles continued to show a significant ($p<.05$) decrease compared to control (4 mast cells/1000 muscle fibers versus 7 mast cells/1000 fibers, respectively).

Mononucleated cells infiltrated the necrotic regions of muscle fibers (Fig. 8). These cells were darkly reactive for acid phosphatase activity, suggesting the presence of lysosome-rich macrophages (Fig. 9).

The protease, tripeptidyl aminopeptidase (TAP), was localized immunohistochemically within Synchronous and Flight AL muscle sections, and serial ATPase sections corroborated fiber types. In the control, SO fibers were moderately immunoreactive for TAP, and the FOG fibers exhibited high reactivity (Fig. 10). Omission of the primary antiserum eliminated this immunostaining (Fig. 11). The SO fibers atrophied to a greater extent than FOG fibers in the Flight AL muscles. The FOG fibers retained high levels of TAP immunoreactivity whereas SO fiber staining ranged from below to above that of the control (Fig. 12).

The SO and FOG fibers in the Synchronous control AL muscles possessed moderate immunoreactivity for ubiquitin conjugates (Fig. 13). Specificity of the immunostaining was verified by leaving out the primary ubiquitin conjugate antibodies (Fig. 14). Immunostaining of atrophic fibers in the Flight AL muscles ranged from diminished to markedly elevated. Fibers manifesting elevated immunofluorescence, were not stained uniformly throughout the sarcoplasm (Fig. 15).

Ultrastructural properties of Flight AL and EDL muscles. The AL and EDL muscles were well preserved and free of fixation artifacts, except for swelling and extraction of mitochondria deep within the tissue block where fixation by immersion was not rapid. For the present study, comparisons of structure were made in the well fixed superficial regions. In addition, the structure of the Flight muscles was more severely affected by spaceflight in the midbelly (endplate) region than the proximal and distal ends. Therefore, comparable regions were compared for Flight and controls when assessing changes. For both the AL and EDL muscles, no detectable differences in morphology were evident between the Synchronous, Vivarium and Basal control groups.

At the ultrastructural level, muscle fiber atrophy and necrosis were evident in the Flight AL muscles (Figs. 16,17). On average, 3.8±.2% of the subsarcolemmal area (3 μm deep) was occupied by subsarcolemmal mitochondria in the Flight muscles compared to 5.5±.2% in the Synchronous controls (Figs. 18,19). This 31% decrease was significant ($p<.005$) and consistent with the observed reduction in peripheral SDH histochemical staining of Flight AL muscle fibers (not illustrated). The content of mitochondria in the A bands of the Flight AL muscles was increased 4 fold compared to the Synchronous control value (0.8±.01% versus 0.2±.04%, respectively, $p<.005$) (Figs. 20,21). A 28% increase in the mitochondrial content of the non-A band was detected (Flight 11.3±1.6% versus Synchronous 8.8±.3%), but this difference was not statistically significant (Figs. 20,21).

Atrophy of the myofibrils of AL Flight muscles was quantitated by measuring the length of the Z lines viewed in longitudinal section (Figs. 22,23). The mean length of Z lines in Flight AL (413±17 nm) was significantly ($p<.005$) less than that of the Synchronous controls (538±7 nm).

Closer to the midbelly region of the Flight AL muscles, the myofibrils were disrupted in addition to being reduced in size (Figs. 24,25). There was longitudinal streaming of the Z bands and loss of sarcomere banding (Fig. 24). In the transition zone from intact myofibrils to complete disruption, the Z bands were reduced to very short, punctate densities (Fig. 25). Other portions of the fiber

lacked thick filaments and exhibited large Z band-like densities on bundles of actin-like filaments (Fig. 25).

Muscle fiber disruption and cellular infiltration. Normal AL muscle fibers of the Synchronous controls contained well organized contractile proteins and peripheral myonuclei (Figs. 16,26). The rich vascularity of the muscle was evidenced by the numerous capillaries surrounding the fibers (Fig. 16). Distributed among the atrophic fibers of the Flight muscles were damaged fibers exhibiting segmental necrosis (Figs. 27,28). The lesions were segmental because in both directions away from the damage site the fiber was intact and exhibited simple atrophy. At the lesion, the cell membrane was violated, and the fiber was invaded by macrophages, neutrophils, occasional eosinophils, and other, as yet unidentified, mononucleated cells (Figs. 17,27,29,30).

Some necrotic fibers contained large cells, rich in ribosomes, suggestive of myoblasts initiating regeneration (Fig. 30,31). These putative regenerating myoblasts were most likely derived from activated satellite cells. In the control muscles, the satellite cells were unremarkable; they occupied a pocket between the basal lamina and muscle cell membrane (Fig. 32). They appeared dormant, possessing little cytoplasm and containing a nucleus with highly condensed chromatin. In contrast, satellite cells associated with intact fibers in the necrotic regions of Flight muscles showed signs of active growth; the cytoplasm was increased and filled with ribosomes, rough endoplasmic reticulum, and hypertrophied golgi complexes (Fig. 33). Compared to the Synchronous controls, there was a significant ($p<.05$) increase (47%) in the number of satellite cell nuclei that were euchromatic and contained enlarged nucleoli. A similar trend was found for myonuclei. There was a 39% increase in hypertrophied myonuclei which were larger, possessed less heterochromatin, and contained more extensive nucleoli than controls (Figs. 34,35).

Characterization of mononuclear cells and edema. The fixed-tissue macrophages of control AL muscles showed little phagocytic activity. The nucleus was small and condensed, the cytoplasm was sparse with few phagocytic vacuoles, and cell processes were not elaborate (Fig. 36). In contrast, macrophages in the Flight AL muscles, especially within and near damaged regions, were enlarged, exhibited profuse phagocytic activity, and numerous cell processes (Fig. 27,37). They often assumed elongated shapes suggestive of migration along and into damaged muscle fibers. The other major invading cell was the polymorphonuclear neutrophil (Baggiolini, 1980) (Fig. 38). As with macrophages, neutrophils engaged in phagocytosis (Figs. 27,30,39,40). Eosinophils, easily recognized by their oval granules, were rare, but occasionally found within necrotic fibers (Fig. 39). An ultrastructural tally of the mononucleated cells, based strictly on morphological characteristics, indicated that up to 70% were macrophages, up to 29% were neutrophils, and 1% or less were eosinophils, mast cells and unidentified cell types. Immunological cell markers are needed to classify cell types with certainty (Engel & Arahata, 1986).

The extracellular matrix showed increased electron density of a particulate and fibrillar nature in the damaged regions of Flight AL muscles. It appeared that proteins derived from the blood and fragmented muscle fibers permeated the interstitium and caused edema (Figs. 5,6,17,27,29,30,38,40). Extravasated erythrocytes implied breakdown of the microcirculatory vessels (Figs. 27,30,39,40). Disruption of the endothelial cells of capillaries, venules and small arterioles was common in the damaged regions (Fig. 41).

Neuromuscular junctions in control and flight muscles. The neuromuscular junctions of control AL muscles consisted of motor nerve terminals nestled over primary and secondary synaptic clefts of the postjunctional membrane (Fig. 42). A dense basement membrane filled the synaptic cleft, separating the motor nerve terminals and the postjunctional membrane. Nerve terminals were capped by Schwann cell processes on the side away from the muscle fiber. Numerous synaptic vesicles filled the terminals. The neuromuscular junctions on intact fibers in the AL muscles of Flight animals exhibited an equal mixture of normal and degenerating terminals (Figs. 43-46). Degenerating nerve terminals contained few synaptic vesicles, but there was an abundance of

membranous and filamentous debris (Figs. 44-46). Schwann cell processes insinuated between the severely damaged terminals and the postjunctional basement membrane. Often in the vicinity of degenerating terminals, expanses of postjunctional membrane were not contacted by nerve elements (Fig. 45). These morphological relationships are characteristic of axon degeneration and denervation of the muscle fibers (Riley, 1981). In contrast to the junctions in the Flight AL muscles, those in the Flight EDL muscle fibers were indistinguishable from controls (Fig. 47).

Inspection of the intramuscular nerve bundles revealed that the nerve degeneration involved more than the nerve terminals. The nerve bundles in the non-damaged portions of the Flight AL muscles appeared normal; they contained myelinated and nonmyelinated axons separated by perineurial bundles of collagen (Fig. 48). Nerve bundles in the damaged regions often showed clumping and diminution of the neurofilaments and microtubules within the axons (Fig. 49). More striking was the apparent extraction and dissolution of the perineurial collagen bundles, suggestive of collagenase activity (Figs. 49,50). In some disrupted nerve bundles, small clusters of naked nerve processes, abutting the schwann cell, were indicative of nerve fiber regeneration (Fig. 50).

The ultrastructure of the Flight EDL muscles was not distinguishable from the controls. The macrophages and satellite cells were in the resting states (Figs. 51,52). The microcirculatory vessels were intact. There was no interstitial edema or extravasation of erythrocytes (Fig. 53). Neutrophils were not encountered in the interstitium. The myofibrils and mitochondria of the SO, FOG and FG fibers appeared normal (Figs. 54-56). As in controls, SO fibers possessed medium-sized mitochondria nearly completely confined to the I bands (Fig. 54). The mitochondria in the FOG fibers were larger and present in both the I and A bands (Fig. 55). The FG fibers contained low numbers of small mitochondria residing mainly in the I bands (Fig. 56).

Biochemical assays. The biochemical results and discussion are described in Dr. Eliis's final report (Part II).

CONCLUSIONS

The present study demonstrates that skeletal muscle weakness associated with prolonged spaceflight is complex, resulting from more than simple muscle fiber shrinkage (atrophy). Reduction of muscle strength may result from a combination of simple muscle fiber atrophy, muscle fiber segmental necrosis, degeneration of the motor innervation, and disruption of the blood supply. The present Cosmos 1887 findings are consistent with previous spaceflight reports (Ilyina-Kakueva et al., 1976; Baranski et al., 1979; Castleman et al., 1978; 1981; Rokhlenko & Savik, 1981; Martin & Edgerton, 1985; Ilyina-Kakuyeva, 1987; Riley et al., 1987). The weightbearing antigravity muscles (AL, Sol, and Plt) atrophied more than the nonweightbearing EDL muscle. Ranking mean percentage of muscle fiber atrophy from greatest to least puts Sol 38% & AL 36% > Plt 21% > EDL 16%. This differential atrophy is partly explained by the fiber type makeup of the muscle, and differing degrees of fiber type atrophy which occurs SO > FOG > FG. The AL and Sol are mostly composed of SO fibers whereas FG and FOG predominate in the EDL. Thus, the degree of spaceflight- induced atrophy is muscle fiber type specific.

More restrictive than atrophy was the occurrence of the muscle fiber, nerve, and vascular pathologies which only involved the AL and Sol. Within the AL, the degree of pathology was not uniform throughout. The midbelly or endplate region was more extensively damaged, and the destruction was more advanced than either end of the muscle, suggesting that the initial lesions occurred in the middle and spread towards the ends. Since the muscle fibers span the entire length of the muscle, the regional susceptibility cannot be explained by muscle fiber population differences. The basis for this regional heterogeneity is unknown, but studies are continuing to identify unique characteristics that may account for the phenomenon. The greater disruption in the midbelly cannot be explained by excessive shortening of the muscle during spaceflight because

tenotomy, which permits hypershortening, generates segmental necrosis preferentially at the ends of the muscle (Baker, 1983).

Another type of regional difference in the Flight AL muscles correlated with fiber type composition. The rostral half of the AL, composed of both SO and FOG fibers, exhibited less atrophy and damage than the caudal half, predominantly SO fibers. These fiber types were defined by the histochemical myofibrillar ATPase reaction. Recent studies by Hoh and coworkers (Hoh & Hughes, 1988; Hoh et al., 1988) using isomyosin antibodies suggest that there are genetically distinct subtypes of the three basic fiber types not resolved histochemically. Furthermore, these subtypes exhibit differential atrophy following denervation. Consideration of the regional heterogeneity within a skeletal muscle will be even more important when investigating the effects of spaceflight on primates, including humans, which have larger muscles. Choice of biopsy sites could greatly affect the types and extent of changes seen.

The increased myofibrillar ATPase histochemical activity in SO fibers of AL muscles indicated that they were acquiring fast fiber properties during the 12.5 day mission. If the transformation was complete, the mitochondrial content should decrease. While subsarcolemmal mitochondrial content and peripheral SDH histochemical staining were reduced, intermyofibrillar mitochondria were unchanged or somewhat elevated. These observations are consistent with Dr. Edgerton's quantitative measurements of SDH activity of Flight Sol muscles from the same rats. Similar results were obtained previously for the Sol muscle fibers of the Spacelab-3 Flight rats (Riley et al., 1987). It appears that subsarcolemmal mitochondria are selectively reduced whereas the progressive breakdown of myofibrils maintains the relative intermyofibrillar mitochondrial concentration near normal. These findings indicate the red AL and Sol will not show increased contractile fatigability which is characteristic of FG fibers. However, the reduction of subsarcolemmal mitochondria should affect energy-requiring processes associated with the cell membrane, such as the transport of ions and metabolites.

The Sol muscle fibers of Spacelab 3 rats exhibited focal losses of myofilaments from the margins and central portions of myofibrils (Riley et al., 1987). Since the atrophy was more severe in the present mission, the focal loss of myofilaments was expected to be more pronounced. However, the focal deletions were unremarkable. Perhaps, the two-day postflight period of muscle contractile activity caused synthesis and restoration of myofilaments. The hypertrophy of myonuclei, accompanied by enlarged nucleoli and increased euchromatin, is consistent with elevated protein synthesis. Muscles harvested immediately upon landing, to minimize the early readaption to gravity, are needed to assess whether focal lysis of myofibrils is progressive.

The selective loss of contractile proteins during disuse atrophy has not been satifactorily explained (Guba et al., 1977; Riley et al., 1988a). Recently, we proposed that ubiquitination of contractile proteins enhances their susceptibility to proteolysis (Rechsteiner, 1987; Haas, 1988; Riley et al., 1988a). Ubiquitination and TAP activity were increased in the atrophic muscles of Spacelab 3 rats and those undergoing atrophy during hindlimb unloading by tail suspension (Fitts et al., 1986; Riley et al., 1986; Riley & Haas, unpublished observations). The AL muscles from the present animals were not large enough to perform biochemical measures of ubiquitin pools and TAP activity. Immunostaining for TAP did not provide a clear indication of an increase in the protease in the Cosmos 1887 muscles. However, elevated immunofluorescence staining for ubiquitin conjugates was consistent with increased ubiquitination of muscle proteins during spaceflight-induced muscle atrophy.

As striking as the marked atrophy of the AL and Sol muscle fibers of the Cosmos 1887 rats was, the extensive segmental necrosis was more dramatic, involving 2 to 5% of the fibers in 4 Flight rats (no.s 6,7,8,10) and 24% in the fifth rat (no. 9). Interestingly, for 4 of 5 rats there was a direct correlation between the percentage of damaged fibers and the degree of atrophy in the AL. Why rat no. 9 was the most severely affected by spaceflight should be better understood when the effects

on other body systems are compared at the Cosmos Final Report Symposium in Moscow. While the changes in muscles during spaceflight are expected to be predominantly influenced by a reduced workload and decreased contractile activity, extrinsic systemic factors, such as hormonal and immunological, should be considered.

Segmental lesions represent portions of the muscle fibers destroyed when the cell membrane is violated. It is necessary to perform additional studies to identify the primary cause of membrane disruption. There are a number of possible scenarios to explain some of the observations. For example, leakage of muscle cell contents could have activated and attracted macrophages as well as neutrophils into the lesioned site where they participated in phagocytosis. Many unidentified mononuclear cells were also present; since determining the identities of these cells would aid in understanding the mechanism of muscle necrosis, future experiments will employ immunomarkers as described by Engel and Arahata (1986). The milieu surrounding damaged fibers generally was edematous. Release of cell contents stimulates mast cell degranulation and the release of histamine which promotes edema by increasing vascular permeability (Schwartz & Austen, 1984). Degranulated mast cells were uncommon; however, the number of toluidine blue-positive mast cells was lower in the Flight AL muscles. Mast cells may have secreted during flight or landing and contributed to the muscle edema.

One identified cause of edema was breakdown of the endothelial cells of the microcirculatory vessels which leaked erythrocytes into the interstitium. Destruction of capillaries was reported for previous Cosmos missions and following restricted-movement hypodynamia (Portugalov et al., 1971; Portugalov & Ilyina-Kakueva, 1973; Ilyina-Kakueva et al., 1976; Roknlenko & Savik, 1981; Ilyina-Kakuyeva & Portugalov, 1981; Ilyina-Kakuyeva, 1987). It was hypothesized that during reduced muscle contractile activity there is congestion of blood flow in the muscle and loss of vascular tone. This results in ischemia and anoxia that damages the muscle cell membranes (Maki et al., 1986). The edema and endothelial necrosis was limited to the highly vascularized AL and Sol muscles. This is reasonable because these muscles function primarily on oxidative metabolism making them more susceptible to oxygen deprivation than the Plt and EDL which can compensate by anaerobic glycolysis (Maki et al., 1986). Interestingly, vascular occulsion produces muscle fiber necrosis more common in the middle of the Plt muscle, and the susceptibility of fiber types to ischemic damage is SO > FOG > FG (Maki et al., 1986). The vascular pattern was the primary factor in determing the distribution of ischemic changes. The distribution of the blood vessels in the AL muscles is one of the features being examined that may account for the higher incidence of segmental necrosis in the midbelly.

The type of muscle fiber destruction present in the Flight AL muscles is very similar to that reported for eccentric strenuous exercise (Armstrong et al., 1983; Salminen & Vihko, 1984; Ogilvie et al., 1988). Weightbearing lengthening contractions appear to disrupt the muscle fiber membrane and cause segmental necrosis within one or two days after exercising. Since the Flight rats with debilitated antigravity muscles were exposed to the increased workload of gravity for 2 days before sacrifice, it is possible that some of the pathological changes resulted from postflight "strenuous exercise". This can be assessed by analyzing muscles removed immediately upon landing. Some damage may occur during spaceflight because Sol muscles harvested 4.5 to 9 hours after landing possessed necrotic muscle fibers (Roknlenko & Savik, 1981; Ilyina-Kakuyeva, 1987). Inflight and postflight conditions may generate similar neuromuscular pathologies, as the tissue has a limited repetoire of responses to injury. Postflight stress may exacerbate the inflight changes. Regardless of when the damage occurred, it is important to recognize that pathological changes result from spaceflight and effective countermeasures to reduce this damage must be found.

Destruction of the motor innervation produces muscle weakness because denervated muscle fibers are not activated. In the Flight AL muscles, approximately 14% of the neuromuscular junctions examined had their motor nerve terminals disrupted. The nerve damage involved preterminal

axons as well. Degenerating terminals had fewer synaptic vesicles, and the axon cell membrane was violated. In the worst cases, the damaged terminals were engulfed and degraded by hypertrophied schwann cells with increased lysosomes. The morphological changes were similar to those seen following axotomy (Riley, 1981). Similar destruction of nerve terminals was reported for Cosmos 936 (Baranski et al., 1979). They postulated that reduced neural activity during spaceflight produced the terminal degeneration. A primary defect in the axon is possible because, in the present study, damaged junctions were observed on intact muscle fibers. This suggests that the nerve lesions were not secondary to destruction of the muscle fibers.

Early signs of regeneration were detected in both damaged muscle fibers and nerves. Myoblast-like cells were present in the segmental necrotic lesions cleared of cell debris. The source of these myoblasts is most likely activated satellite cells which were more prevalent in the damaged Flight AL muscles. Bischoff has demonstrated that crushed muscle fibers release a soluble factor that stimulates satellite cell mitosis (Bischoff, 1986a,b). In the present study, there was a direct correlation between the distributions of hypertrophied satellite cells and segmental necrosis. Activated satellite cells in nondamaged regions are capable of migrating into the damaged fibers (Schultz et al., 1985). Promoting muscle fiber regeneration by injecting a satellite cell mitogenic factor may facilitate repair of muscle during spaceflight.

Following distal destruction of an axon, the axon dies back to some extent and then initiates regrowth within a day or two (Riley et al., 1988b). The presence of naked fine nerve processes along the schwann cells of small intramuscular nerve bundles, in which most of the myelinated axons were missing, suggests that nerve regeneration was in progress. Functional reinnervation of the endplates should occur rapidly because the axons can follow the schwann cells back to the junctions. These results indicate that if similar nerve damage occurred in human muscles during spaceflight, there might be reinnervation and recovery of strength without the pathological process being detected unless biopsies were taken.

In the present study, the onset of regeneration of both muscle and nerve fibers was detected postflight. There is previous evidence that restoration would have resulted, if the Flight animals had been allowed to survive (Ilyina-Kakueva & Portugalov, 1977). It must be remembered, however, that human muscles and nerves generally do not regenerate as rapidly or as completely as rodent muscles. Scarring and partial denervation of human muscle may result and produce a permanent weakness.

That humans may manifest pathological changes as well as simple atrophy during spaceflight is supported indirectly by recent ultrastructural findings showing disrupted capillaries in soleus muscles following 30 days of head down bedrest (Hikida & Dudley, 1988). During long term spaceflight, simple atrophy may be reduced by exercise, but repair of necrosis of muscle fibers, motor axons, and blood vessels would be dependent upon the effectiveness of complex processes of regeneration. There is ground-based evidence to expect that regeneration may be compromised in space because of the reduction in active muscle tension and exposure of the dividing stem cells to high energy radiation (Denny-Brown, 1951; Ilyina-Kakueva & Portugalov, 1977; Benton et al., 1978; Kovalev, 1983; Gulati, 1987). These issues should be addressed in future missions.

ACKNOWLEDGMENTS

We gratefully acknowledge the dedication and expert assistance of the NASA and Soviet workers who collaborated to obtain the excellent specimens used in this study.

REFERENCES

1. Armstrong, RB, Ogilvie, RW, Schwane, JA. 1983. Eccentric exercise-induced injury to rat skeletal muscle. J. Appl. Physiol. 54:80-93.

2. Baggiolini, M. 1980. The neutrophil. Handbook of Inflammation 2: The Cell Biology of Inflammation. Weissmann, G. Ed. Elsevier/North Holland pp.163-187.

3. Baker, JH. 1983. Segmental necrosis in tenotomized muscle fibers. Muscle & Nerve 6:29-39.

4. Baranski, S, Baranska, W, Marciniak, M, Ilyina-Kakueva, EI. 1979. Ultrasonic ("Ultrastructural") investigations of the soleus muscle after space flight on the Biosputnik 936. Aviat. Space Environ. Med. 50:930-934.

5. Benton, EV, Peterson, DD, Marenny, AM, Popov, VI. 1978. HZE particle radiation studies aboard Kosmos 782. Health Physics 35:643-648.

6. Bischoff, R. 1986a. A satellite cell mitogen from crushed adult muscle. Devel. Biol. 115:140-147.

7. Bischoff, R. 1986b. Proliferation of muscle satellite cells on intact myofibers in culture. Devel. Biol. 115:129-139.

8. Castleman et al. 1978. Spaceflight effects on muscle fibers:Final Reports of U.S. Experiments Flown on Soviet Satellite Cosmos 936. Rosenzweig, SN. Souza, KA. Eds. NASA Technical Memorandum 78526 pp. 224-289.

9. Castleman, KR, Chui, LA, Van Der Meulen, JP. 1981. Automatic analysis of muscle fibers from rats subjected to spaceflight. NASA Technical Memorandum 81289 pp. 267-277.

10. Denny-Brown, D. 1951. The influence of tension and innervation on the regeneration of skeletal muscle. J. Neuropath. Exp. Neurol. 10:94-95.

11. Engel, AG, Arahata, K. 1986. Mononuclear cells in myopathies. Hum. Pathol. 17:704-721.

12. Fitts, RH, Metzger, JM, Riley, DA. 1986. Models of skeletal muscle disuse: a comparison of suspension hypokinesia and hindlimb immobilization. J. Appl. Physiol. 60:1946-1953.

13. Gazenko, OG, Genin, AM, Il'in, YA, Portugalov, VV, Serova, LV, Tigranyan, RA. 1978. Principal results of experiment with mammals onboard the Kosmos-782 biosatellite. Kosmich. Biol. Aviakosmisch. Med. 6:43-[illegible].

14. Guba, F, Meszaros, MG, Takacs, O. 1977. Degradation of myones as a consequence of disuse and denervation. Acta Biol. Med. Germ. 36:1605-1619

15. Gulati, AK. 1987. The effect of X-irradiation on skeletal muscle regeneration in the adult rat. J. Neurol. Sci. 78:111-120.

16. Haas, AL. 1988. Immunochemical probes of ubiquitin pool dynamics. Ubiquitin. Rechsteiner, M. Ed. Plenum Publ. pp.173-206.

17. Hikida, RS, Dudley, GA. 1988. Ultrastructural changes in human skeletal muscle after 30 days of bedrest. Anat. Rec. 220:44A.

18. Hoh, JFY, Hughes S. 1988. Myogenic and neurogenic regulation of myosin gene expression in cat jaw-closing muscles regenerating in fast and slow limb muscle beds. J. Muscle Res. Cell Motil. 9:59-72.

19. Hoh, JFY, Hughes, S, Hale, PT, Fitzsimons, RB. 1988. Immunocytochemical and electrophoretic analyses of changes in myosin gene expression in cat limb fast and slow muscles during postnatal development. J. Muscle Res. Cell Motil. 9:30-47.

20. Ilyin, EA. 1983. Investigations on biosatellites of the Cosmos series. Aviat. Space Environ. Med. Suppl. I 54:S9-S15.

21. Ilyina-Kakuyeva, EI. 1987. Investigation of rat skeletal muscles following short-term spaceflight aboard Cosmos-1667 biosatellite. Kosmich. Biol. Aviakosmich. Med. 21:31-35.

22. Ilyina-Kakuyeva, EI, Portugalov, VV. 1981. Structural changes in the soleus muscle of rats flown aboard the Cosmos series of biosatellites and submitted to hypokinesia. Kosmich. Biol. Aviakosmich. Med. 15:37-40.

23. Ilyina-Kakueva, EI, Portugalov, VV. 1977. Combined effect of space flight and radiation on skeletal muscles of rats. Aviat. Space Environ. Med. 48:115-119.

24. Ilyina-Kakueva, EI, Portugalov, VV, Krivenkova, NP. 1976. Space flight effects on the skeletal muscle of rats. Aviat. Space Environ. Med. 47:700-703.

25. Kovalev, EE. 1983. Radiation protection during space flight Aviat. Space Environ. Med. Suppl. 1 54:S16-S23.

26. Maki, T, Korthals, JK, Prockop, LD. 1986. Distribution of muscle changes in experimental ischemic myopathy. Muscle & Nerve 9:394-398.

27. Martin, TP, Edgerton, VR. 1985. The influence of space flight on the rat soleus. Physiologist 28:379.

28. Ogilvie, RW, Armstrong, RB, Baird, KE, Bottoms, CL. 1988. Lesions in the rat soleus muscle following eccentrically biased exercise. Amer. J. Anat. 182:335- 346.

29. Portugalov, VV, Ilyina-Kakueva, EI. Prolonged space flight and hypokinesia. Aerospace Med. 44:764-768.

30. Portugalov, VV, Ilyina-Kakueva, EI, Starostin, VI, Rokhlenko, KD, Savik, ZF. 1971. Morphological and cytochemical studies of hypokinetic effects. Aerospace Med. 42:1041-1049.

31. Rapcsak, M, Oganov, VS, Szoor, A, Skuratova, SA, Szilagyi, T. 1983. Effect of weightlessness on the function of rat skeletal muscles on the biosatellite Cosmos-1129. Acta Physiol. Hung. 62:225-228.

32. Rechsteiner, M. 1987. Ubiquitin-mediated pathways for intracellular proteolysis. Ann. Rev. Cell Biol. 3:1-30.

33. Riley, DA. 1981. Ultrastructural evidence for axon retraction during the spontaneous elimination of polyneuronal innervation of the rat soleus muscle. J. Neurocytol. 10:425-440.

34. Riley, DA, Allin, EF. 1973. The effects of inactivity, programmed stimulation, and denervation on the histochemistry of skeletal muscle fiber types. Exp Neurol. 40:391-413.

35. Riley, DA, Bain, JLW, Ellis, S, Haas, AL. 1988a. Quantification and immunocytochemical localization of ubiquitin conjugates within rat red and white skeletal muscles. J. Histochem. Cytochem. 36:621-632.

36. Riley, DA, Bain, JLW, Haas AL. 1986. Increased ubiquitin conjugation of proteins during skeletal muscle atrophy. J. Cell Biol. 103:401a

37. Riley, DA, Ellis, S, Bain, JLW. 1982. Carbonic anhydrase activity in skeletal muscle fiber types, axons, spindles, and capillaries of rat soleus and extensor digitorum longus muscles. J. Histochem. Cytochem. 30:1275-1288.

38. Riley, DA, Ellis, S, Slocum GR, Satyanarayana, T. Bain, JLW, Sedlak FR. 1987. Hypogravity-induced atrophy of rat soleus and extensor digitorum longus muscles. Muscle & Nerve 10:560-568.

39. Riley, DA, Sanger, JR, Matloub, HS, Yousif, NJ, Bain, JLW, Moore, GH. 1988b. Identifying motor and sensory myelinated axons in rabbit peripheral nerves by histochemical staining for carbonic anhydrase and cholinesterase activities. Brain Res. 453:79-88.

40. Rokhlenko, KD, Savik, ZF. 1981. Effect of space flight factors on ultrastructure of skeletal muscles. Kosmich. Biol. Aviakosmich. Med. 1:72-77.

41. Salminen, A, Vihko, V. 1984. Autophagic response to strenuous exercise in mouse skeletal muscle fibers. Virch. Arch. Cell Pathol. 45:97-106.

43. Schultz, E, Jaryszak, DL, Valliere, CR. 1985. Response of satellite cells to focal skeletal muscle injury. Muscle & Nerve 8:217-222.

44. Schwartz, LB, Austen, KF. 1984. Structure and function of the chemical mediators of mast cells. Prog. Allergy 34:271-321.

45. Takacs, O, Rapcsak M, Szoor, A, Oganov, VS, Szilagyi, T, Oganesyan, SS, Guba, F. 1983. Effect of weightlessness on myofibrillar proteins of rat skeletal muscles with different functions in experiment of biosatellite Cosmos-1129. Acta Physiol. Hung. 62:228-233.

TABLE 1

PERCENTAGES OF FIBER TYPES IN FLIGHT AND SYNCHRONOUS MUSCLES

Muscle	Percentages of fiber types Flight	Synchronous
Adductor longus		
SO	63±5*	83±1
I	19±3**	1±1
FOG	18±3	16±3
Extensor digitorum longus		
SO	5±1	5±1
FG	37±5	31±2
FOG	58±5	64±2
Plantaris		
SO	10±1	10±1
FG	21±3	24±3
FOG	69±3	66±2

SO - slow twitch oxidative
I - intermediate (putative SO fiber changing to FOG)
FG - fast twitch glycolytic
FOG - fast twitch glycolytic oxidative
* - Flight significantly different from control at $p<.01$
** - Flight different from control at $p<.001$
two tailed Student t test

TABLE 2

FIBER TYPE ATROPHY IN FLIGHT MUSCLES

Muscle	Fiber Cross-sectional Area: Flight	Synchronous	Percent Atrophy
Adductor Longus			
SO	1332±125	2370±121	43.8%**
I	1209±167	1600±148	24.5%
FOG	1854±173	2232±178	17.0%
Extensor Digitorum Longus			
SO	955±77	1157±69	17.4%
FG	2768±290	3170±162	12.7%
FOG	1323±107	1623±58	18.5%*
Plantaris			
SO	1506±67	1919±104	21.5%*
FG	3074±110	4503±333	31.7%*
FOG	1974±80	2364±111	16.5%*
Soleus			
ND	1864±115	3005±100	38.0%**

SO - slow twitch oxidative
I - intermediate (putative SO fiber transforming to FOG fiber)
FG - fast twitch glycolytic
FOG - fast twitch glycolytic
ND - fiber types not distinguishable for soleus (H&E section)
* - percentage atrophy significantly different at $p<.05$
** - percentage atrophy significantly different at $p<.001$
two tailed t-test

TABLE 3

PERCENTAGES OF ABERRANT FIBERS IN ADDUCTOR LONGUS MUSCLES

Group	Normal Fibers	Aberrant Fibers	Mean Total No. Counted	Percentage Aberrant
Flight n=4*	1200±66	45±9	1245±73	3.6±0.6%**
Synchronous n=5	1331±75	2.2±0.5	1333±75	0.17±.04%
Vivarium n=5	1226±85	2.3±0.3	1228±85	0.19±.03%
Basal n=5	1074±134	1.1±0.5	1075±134	0.09±.03%

---

* - The AL muscle of Flignt rat #9 was excluded as a statistical outlier because 24% of the fibers were damaged.

** - The percentage aberrant fibers in the Flight group is significantly different from each of the other three groups ($p < 0.001$; two tailed Student t-test)

Figure 1. An alkaline myofibrillar ATPase stained section of a normal AL muscle from a Cosmos Synchronous control rat. Most fibers are lightly reactive slow twitch oxidative fibers (SO). Darkly stained fast twitch oxidative glycolytic (FOG) fibers are also present. X250.

Figure 2. Following 12.5 days of spaceflight, the AL muscles exhibited overall a 36% fiber atrophy. While all fiber types atrophied, the SO fibers showed the greatest decrease in size. There was an increase in moderately staining fibers which indicated that SO fibers were acquiring myofibrillar ATPase properties of fast fibers. X250.

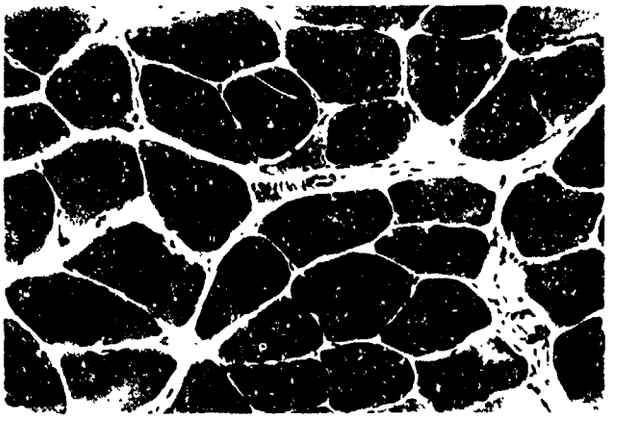

Figure 3. A hematoxylin & eosin (H&E) stained section of an AL Synchronous muscle. The fibers are large, except for the occasional (.02%) small angular fiber (arrow), suggestive of a low rate of spontaneous neurogenic atrophy in normal muscles. X175.

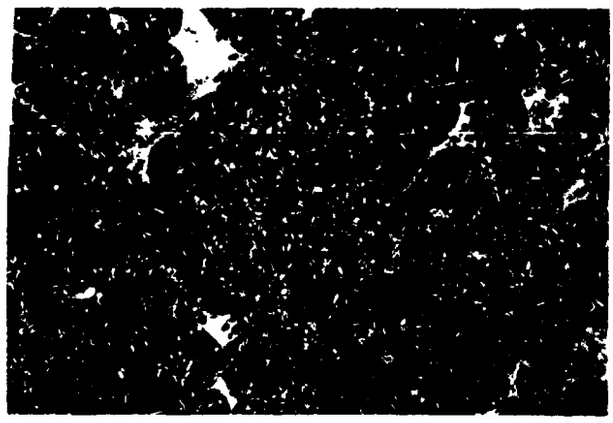

Figure 4. The muscle fibers of the Flight AL are atrophied, and, on average, 3.6% of the fibers exhibit segmental necrosis with invasion by mononucleated cells (arrows). Some lesioned fibers (double arrows) possess a central core of disruption surrounded by intact myofibrils. X175.

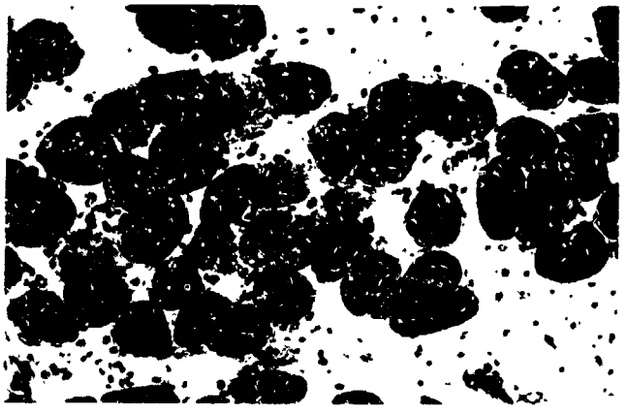

Figure 5. An H&E stained cross section of a Flight AL. The pale staining fibers are undergoing destruction. The edematous extracellular space surrounding the muscle fibers is filled with numerous mononuclear cells. X175.

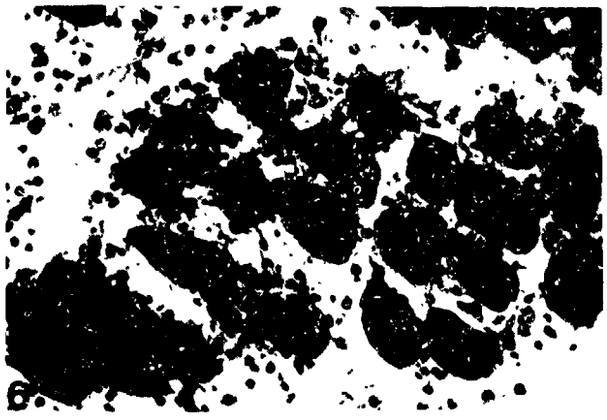

Figure 6. Extensive interstitial edema and mononuclear cell infiltration, as well as muscle fiber necrosis, is present in the Flight soleus muscles. X175.

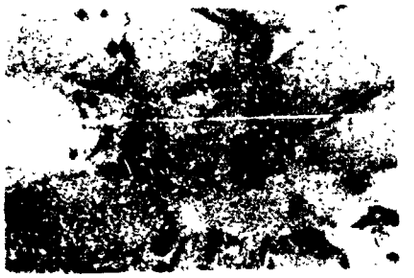

Figure 7. Toluidine blue stained section of a normal AL muscle. Two granule- laden mast cells occupy the perimysial connective tissue. X313.

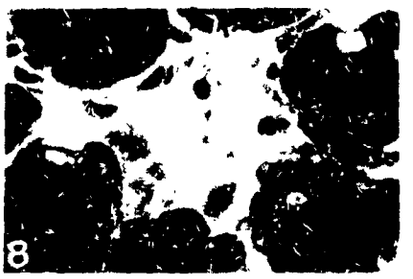

Figure 8. An H&E stained section of a Flight AL. The central necrotic fiber is devoid of myofibrils and filled with mononuclear cells. X400.

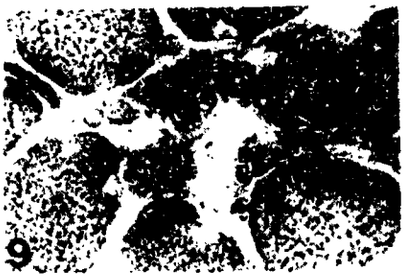

Figure 9. A section, serial to figure 8, stained by acid phosphatase histochemistry reveals that many of the invading cells are darkly reactive, suggestive of high lysosome content. X400.

Figure 10. Indirect immunofluorescence localization of tripeptidyl aminopeptidase (TAP) in a Synchronous AL muscle. The SO fibers show uniformly moderate immunoreactivity, and the six FOG fibers in this section are highly reactive. X145.

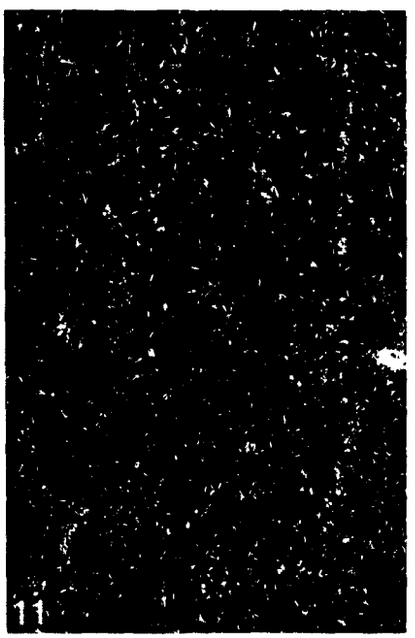

Figure 11. A section serial to that in figure 10. Omission of the primary antiserum eliminates fiber immunostaining, except for autofluorescence of mitochondria at the periphery of the fibers. X145.

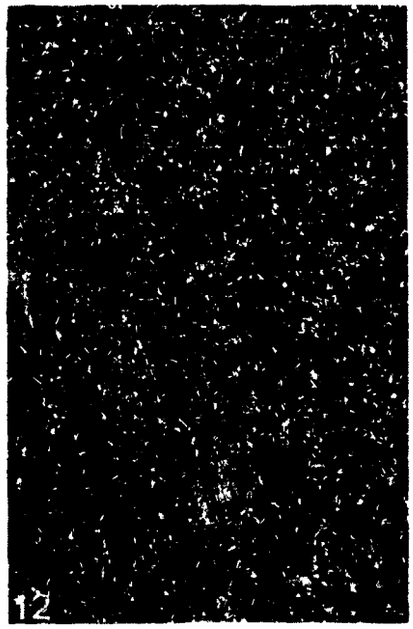

Figure 12. The less atrophic FOG fibers in an AL Flight muscle continue to manifest high levels of TAP immunoreactivity. The more atrophic SO fibers exhibit a range of reactivity from high to low levels of staining compared to the Synchronous control. X145.

Figure 13. Cross section of a Synchronous AL muscle immunostained with ubiquitin conjugate antibodies. Fibers show uniform moderate immunofluorescence. X145.

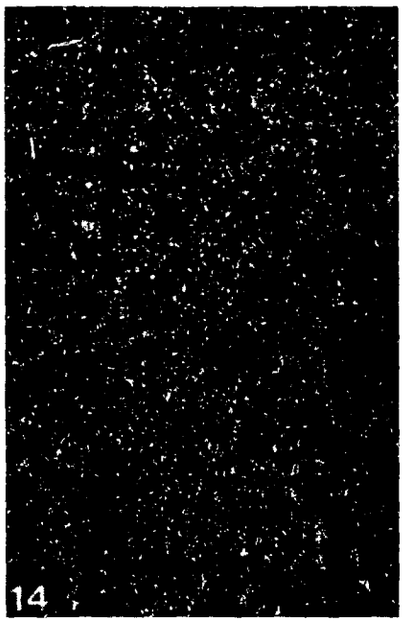

Figure 14. A section serial to that in figure 13. Elimination of the primary antiserum blocks fiber staining, supporting specificity of the antibodies for ubiquitin conjugates. Nonspecific background staining of the subsarcolemmal mitochondria remains. X145.

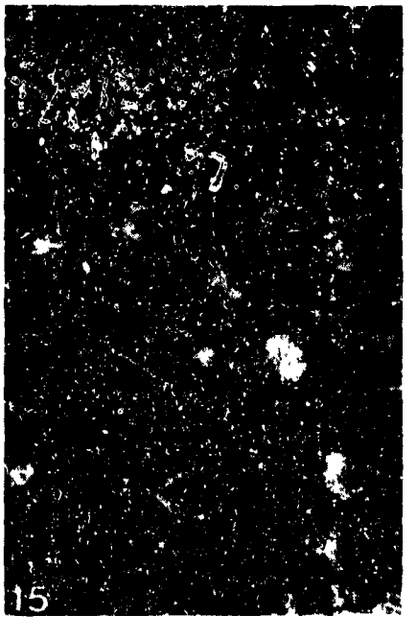

Figure 15. Ubiquitin conjugate antibody staining of atrophic fibers in an AL Flight muscle. Uneven elevated immunofluorescence staining is present in many fibers, indicating regional subcellular increases of conjugates. Other fibers possess uniform staining, ranging from above to below control levels. X145.

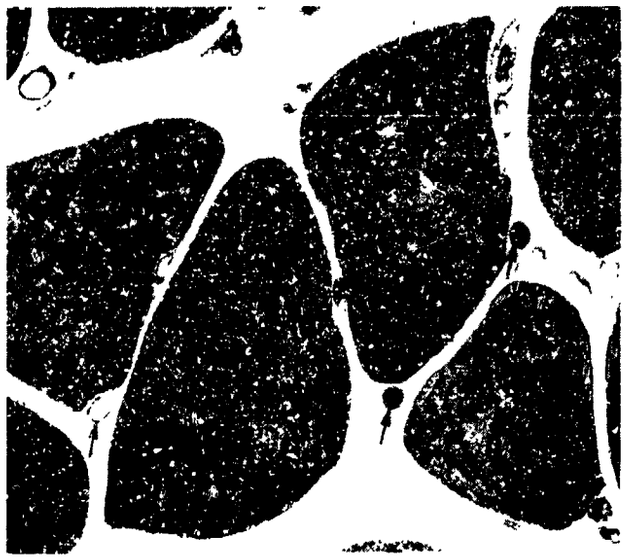

Figure 16. A low magnification electron micrograph illustrating normal muscle fibers in a Basal control AL muscle cut in cross section. Fibers contain well organized contractile proteins and peripheral myonuclei. Capillaries (arrows) occupy the surrounding endomysial connective tissue; some capillaries contain erythrocytes. X840.

Figure 17. Cross section of a Flight AL muscle showing a severely necrotic fiber among the small intact atrophic fibers. The damaged fiber exhibits invasion by macrophages and other unidentified cells. The extracellular matrix is more dense than normal. X840.

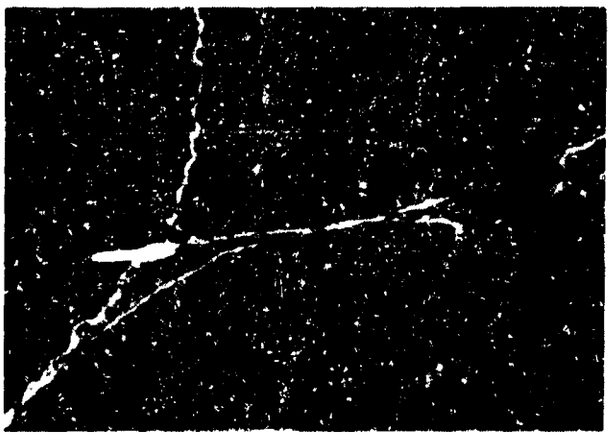

Figure 18. Prominent subsarcolemmal accumulations of mitochondria are present in Synchronous control AL fibers. X5,250.

Figure 19. In the Flight AL muscles, there is a significant reduction in the subsarcolemmal concentration of mitochondria. X5,250.

Figure 20. A cross section of a Synchronous AL muscle fiber illustrates that the majority of the mitochondria encircle the myofibrils at the I band level. Very few mitochondrial profiles are present in the A band. X15,000.

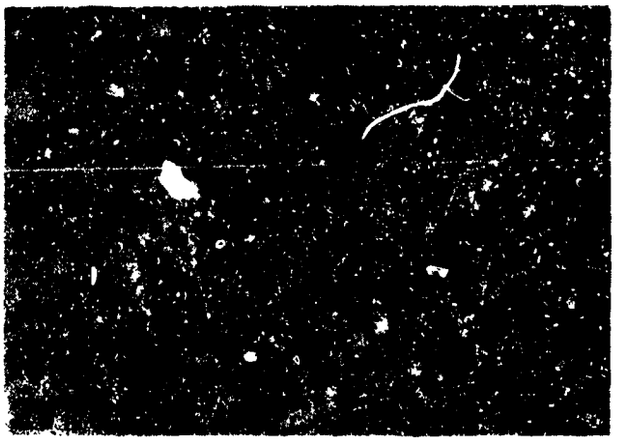

Figure 21. The atrophic Flight AL muscle fibers contain more mitochondria profiles in the A bands than controls. X15,000.

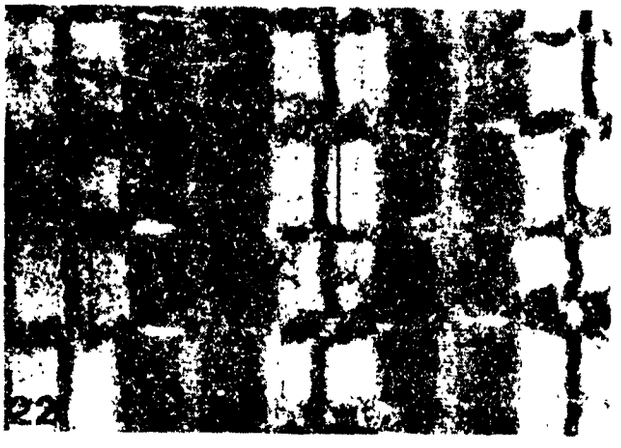

Figure 22. A longitudinal section of a Synchronous AL muscle fiber. The myofibrils are wide with long Z bands (brackets). X14,500.

Figure 23. The myofibrils decrease in diameter in the atrophic Flight AL muscle fibers. The mean Z band length is less than that of controls. X14,500.

Figure 24. Some regions of the atrophic Flight AL muscle fibers exhibit loss of sarcomere structure with longitudinal streaming of the Z bands. X6,750.

Figure 25. In regions of myofibril disorganization, the Z bands (arrows) are extremely short. Areas of this Flight AL in which myofibrils are nearly completely broken down, large Z band-like densities are present (arrowheads). X3,900.

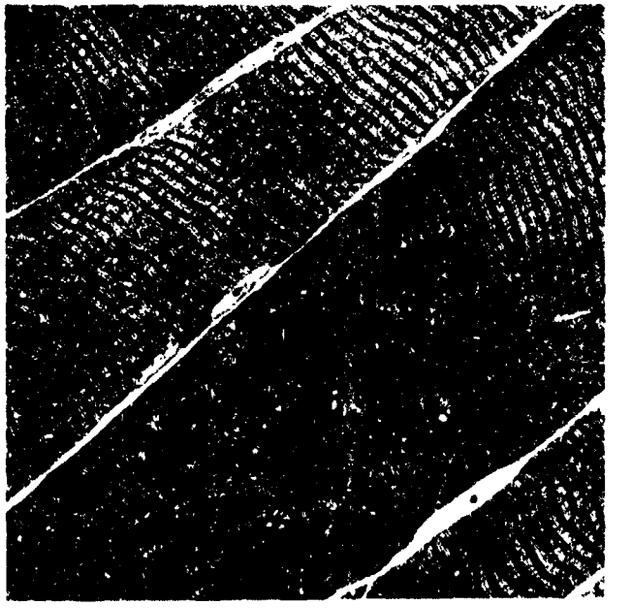

Figure 26. A longitudinal section of AL muscle fibers from a Basal control muscle demonstrating the regular cross striated pattern of the myofibrils. X840.

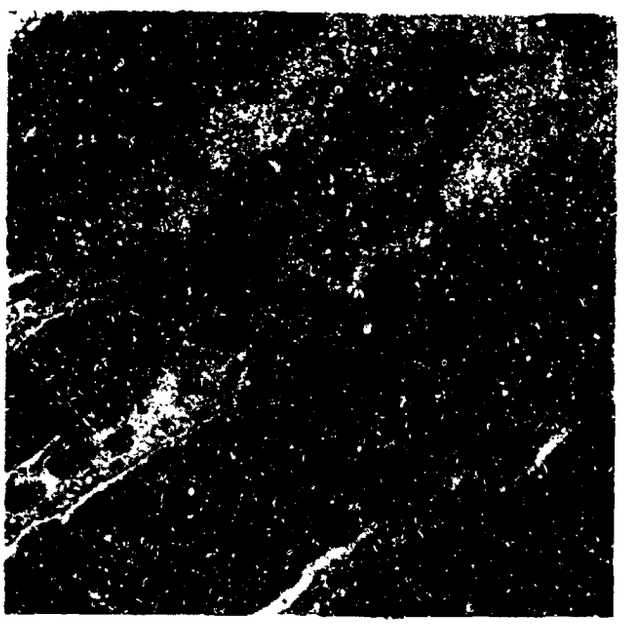

Figure 27. A longitudinal section through the segmental necrotic regions of three muscle fibers in a Flight AL muscle. The plasma cell membranes of the degenerating fibers are disrupted, the contractile proteins form amorphous masses, and fibers are invaded by macrophages (arrows), neutrophils (arrowheads) and other unidentified cell types. Escaped erythrocytes (e) are free in the connective tissue. X840.

Figure 28. A lesioned fiber in a Flight AL muscle. This fiber illustrates the transition from partially disrupted myofibrils leading to a supercontracted mass which borders the segmental necrotic region completely devoid of intact contractile elements. X840.

Figure 29. A cross section of a contraction clot in a necrotic AL Flight muscle fiber. The clot in the right half of this figure is invaded by two macrophages engulfing cellular debris. X2,900.

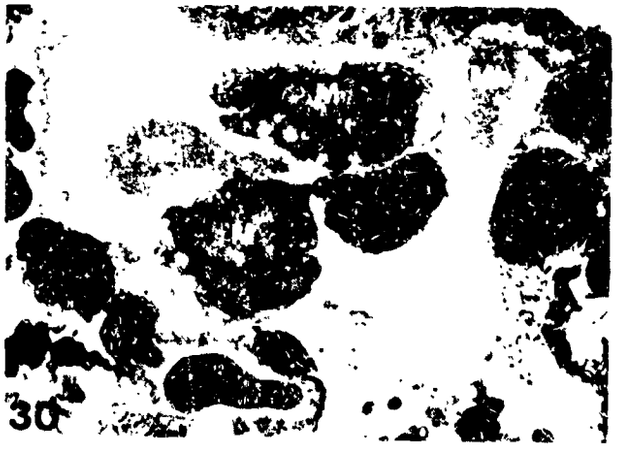

Figure 30. An advanced stage of breakdown of the contractile material within a segmental necrotic region of a Flight AL fiber viewed in cross section. The muscle fiber basal lamina surrounds two macrophages (M) and portions of two regenerating myoblasts (Mb). X2,800.

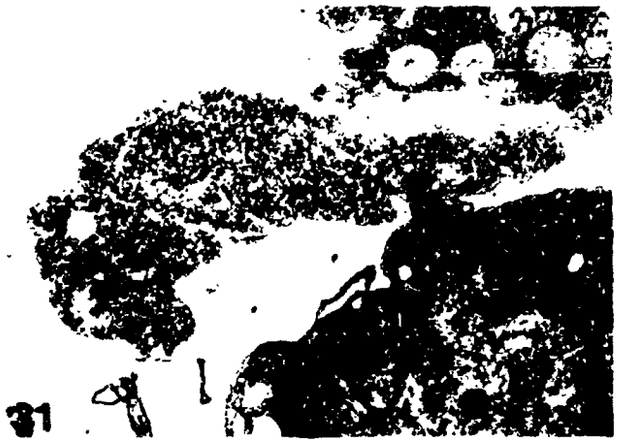

Figure 31. A higher magnification of the regenerating myoblast in figure 30 reveals the ribosome-rich cytoplasm of the growing cell. X8,400.

Figure 32. A quiescent satellite cell on a normal fiber in a Basal control AL muscle. The nucleus is heterochromatic, the nucleolus is not prominent, and the cytoplasm is sparse and contains few organelles. X8,125.

Figure 33. An activated satellite cell on an intact atrophic fiber in an AL Flight muscle. The amount of cytoplasm is greatly increased and electron lucent. There are many ribosomes, rough endoplasmic reticulum, golgi membranes and vesicles. The nucleus exhibits more euchromatin and an enlarged nucleolus indicative of elevated protein synthetic activity. X8,125.

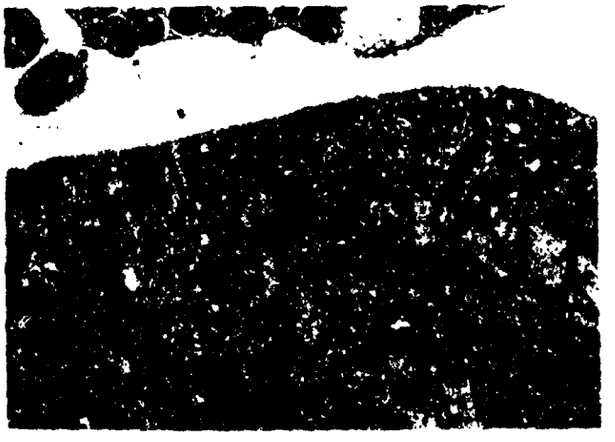

Figure 34. The edge of a Basal control AL muscle fiber. The peripheral myonucleus exhibits marginal heterochromatin and a small nucleolus. In the adjacent connective tissue, a mast cell is releasing secretory granules. Active mast cell secretion was rarely observed in control and Flight muscles. X9,750.

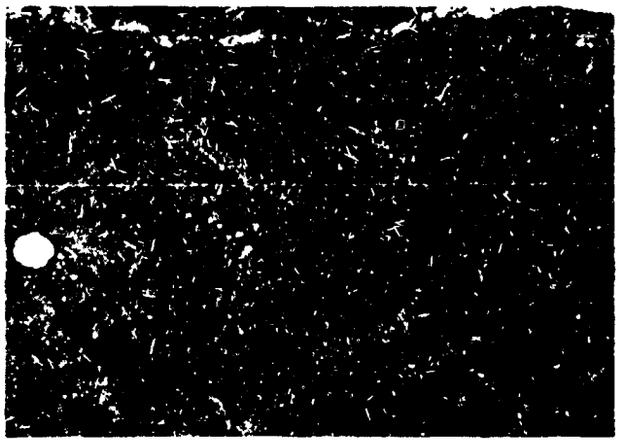

Figure 35. Approximately 40% of the myonuclei examined in the Flight AL muscle fibers showed increased euchromatin and hypertrophied nucleoli. X9,750.

Figure 36. A quiescent tissue macrophage in a Synchronous AL muscle. The nucleus is heterochromatic, the cytoplasm is dense and filled with lysosomes, and cell processes are few in number. X9,600.

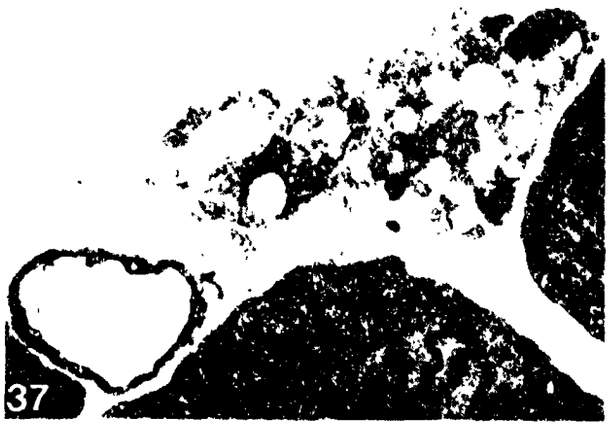

Figure 37. Activated macrophages are very common in the Flight AL muscles. They exhibit enhanced phagocytosis of extracellular material. Not visible in this section is the nucleus which is more euchromatic and contains a larger nucleolus than normal. X5,750.

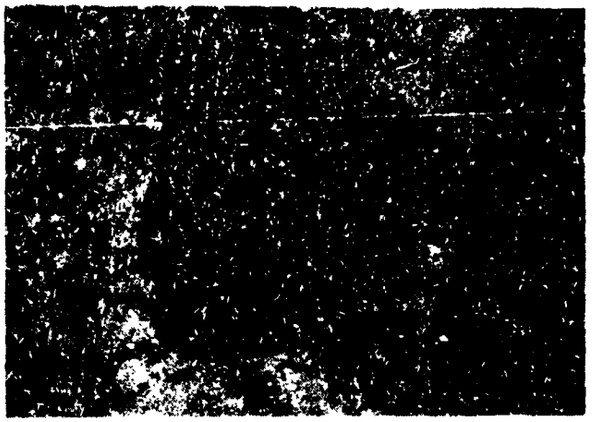

Figure 38. Invasion of Flight AL muscles by polymorphonuclear neutrophils is common in regions of muscle fiber necrosis. The neutrophil is characterized by a multilobed nucleus and dense cytoplasm. In this figure, the electron dense material surrounding the neutrophil is most likely blood serum proteins that escaped from damaged capillaries. X8,710.

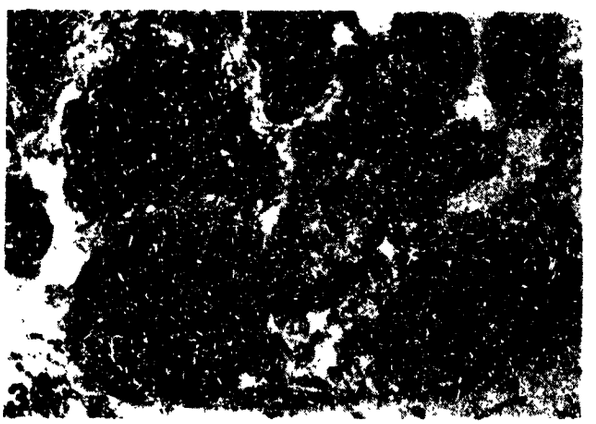

Figure 39. Flight AL muscle. Eosinophils (E) occasionally participated in the invasion of necrotic muscle fibers. A macrophage (M) with an ingested erythrocyte (R) is also present. The identities of the other mononuclear cells are uncertain. X5,625.

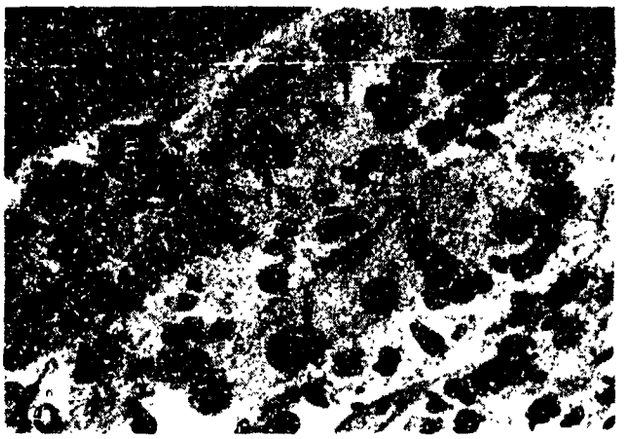

Figure 40. Extravasation of erythrocytes (E) into the connective tissue was common in the necrotic regions of Flight AL muscles. Macrophages (arrows), neutrophils (arrowheads, and other unclassified mononuclear cells fill the damaged region of the muscle. X750.

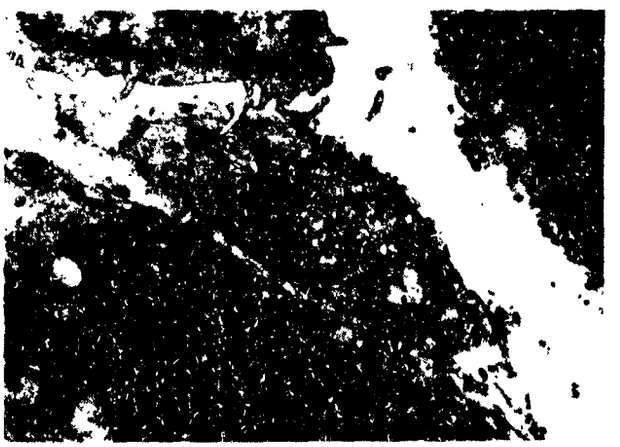

Figure 41. In the damaged regions of Flight AL muscles, many microcirculatory vessels were disrupted. A degenerating endothelial cell of a capillary is shown (D). Another endothelial cell appears intact. It is filled with pinocytotic vesicles (P). X8,375.

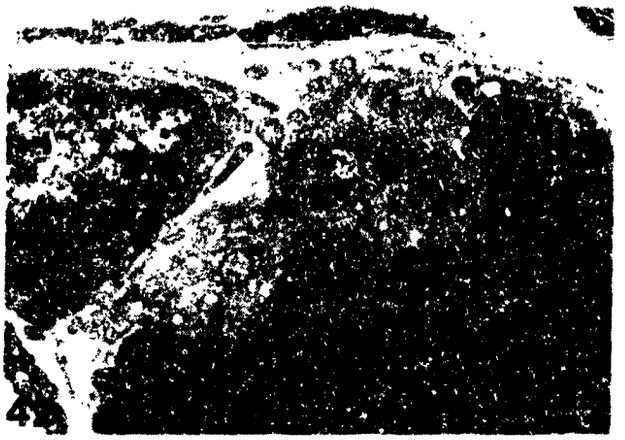

Figure 42. A normal neuromuscular junction on an AL muscle fiber in a Basal control rat. Synaptic vesicle-laden terminals are separated from the postjunctional muscle membrane by a prominent basement membrane which fills the primary and secondary synaptic clefts. X8,375.

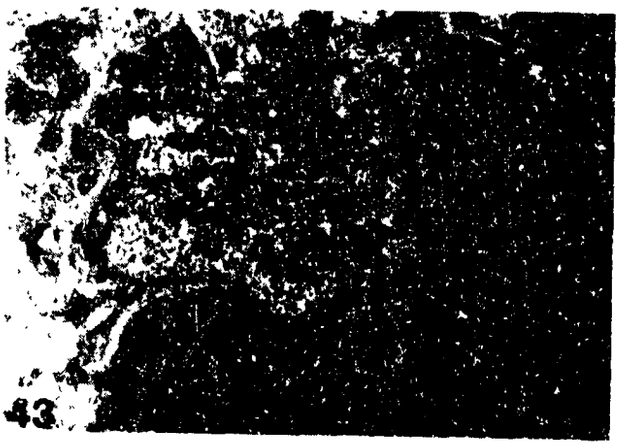

Figure 43. A normal appearing neuromuscular junction on an intact AL Flight muscle fiber. The nerve terminal is filled with synaptic vesicles. Schwann cell processes cap the side of the terminal away from the postjunctional membrane. X9,213.

Figure 44. A disrupted motor nerve terminal in a Flight AL muscle. There are fewer synaptic vesicles. Schwann cell processes partially separate the terminal and the postjunctional membrane. X9,213.

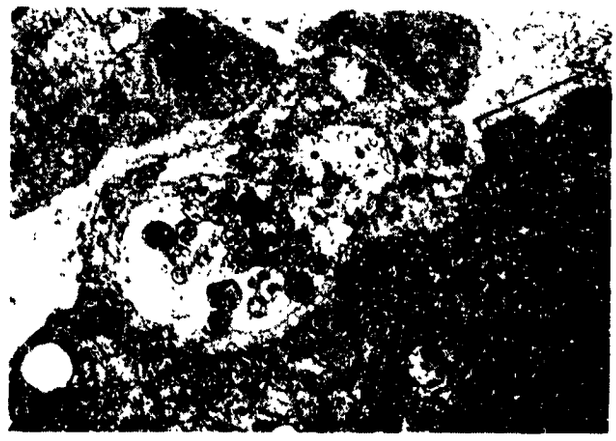

Figure 45. A more severely disrupted neuromuscular junction on an intact muscle fiber from a Flight animal. Very few synaptic vesicles are present and the axolemma appears broken. Schwann cell processes are completely interposed between the terminal and the postjunctional membrane. An adjacent area of the postjunctional membrane (bracket) is devoid of nerve elements. X9,213.

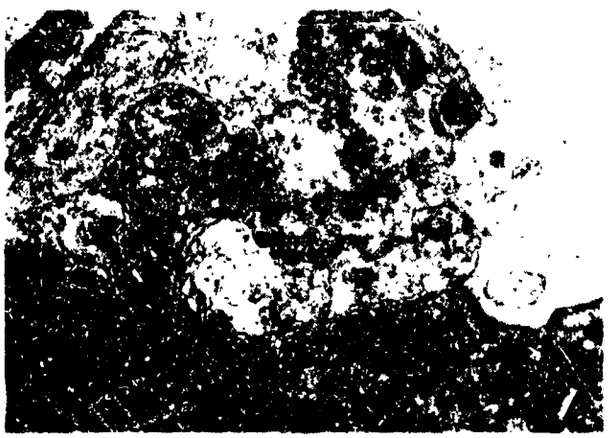

Figure 46. The nerve terminals of this degenerating neuromuscular junction in a Flight AL muscle lack synaptic vesicles and mitochondria and the axolemma is not intact. The schwann cell is hypertrophied and abuts the postjunctional membrane, presumably vacated by degenerated terminals. X9,213.

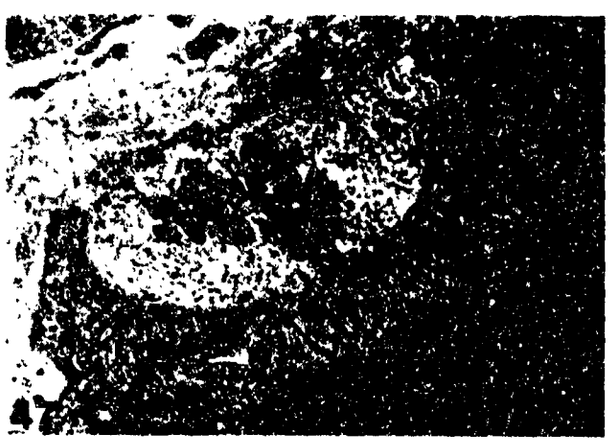

Figure 47. As illustrated here, the neuromuscular junctions of the Flight EDL muscles were normal in appearance. X13,200.

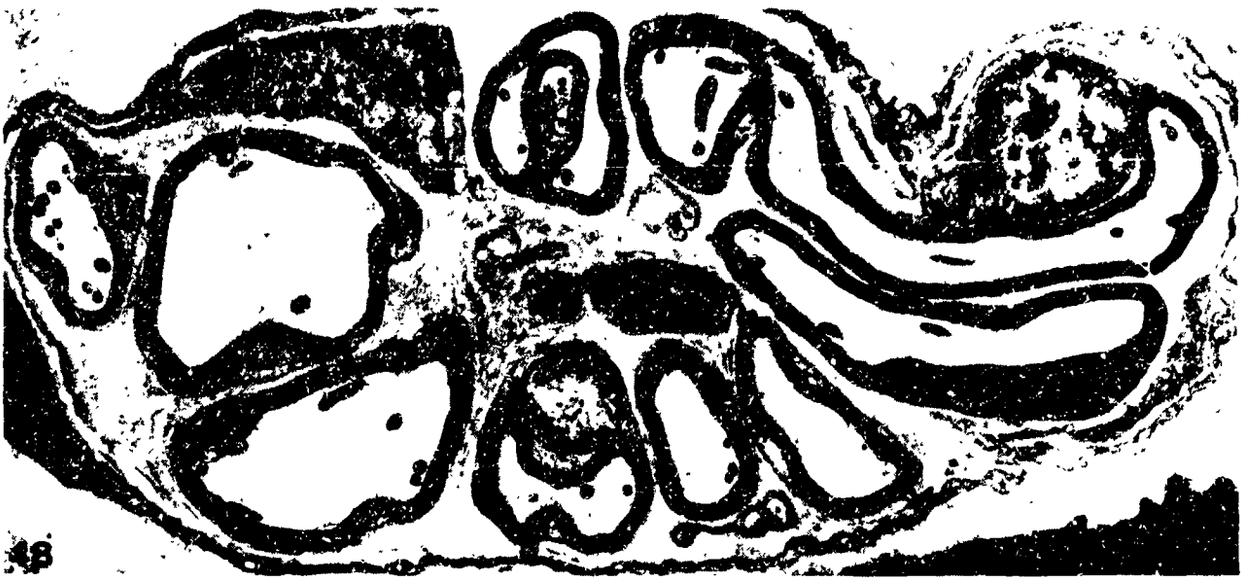

Figure 48. A large intramuscular nerve bundle in a nondamaged region of a Flight AL muscle. The nerve bundle is similar in appearance to those in control muscles. The myelinated and nonmyelinated axons have intact cell membranes. The axons contain neurofilaments, microtubules, and mitochondria. The perimysial connective tissue has prominent bundles of collagen which fill the regions between schwann cells. X6,188.

Figure 49. A portion of an intramuscular nerve bundle in a damaged region of a Flight AL muscle. The collagen bundles between schwann cells are extracted and markedly reduced in size. The neurofilaments and microtubules are clumped (arrow) and reduced in amount. Mitochondria appear swollen and disrupted. X6,188.

Figure 50. A small intramuscular nerve bundle in a necrotic region of a Flight AL muscle. A trio of fine nerve processes (arrow) contact the large central schwann cell. This suggests axon regeneration. The two myelinated axons appear normal. The perineurial collagen bundles are extracted. X6,188.

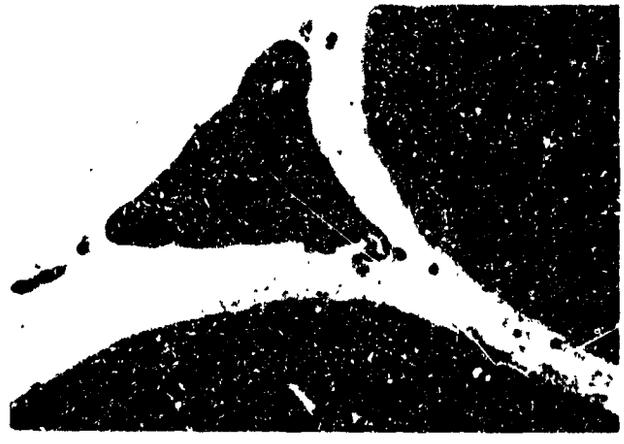

Figure 51. A resting fixed-tissue macrophage in a Flight EDL muscle. The nucleus is heterochromatic, there is little cytoplasm, and the cell has few processes. X13,000.

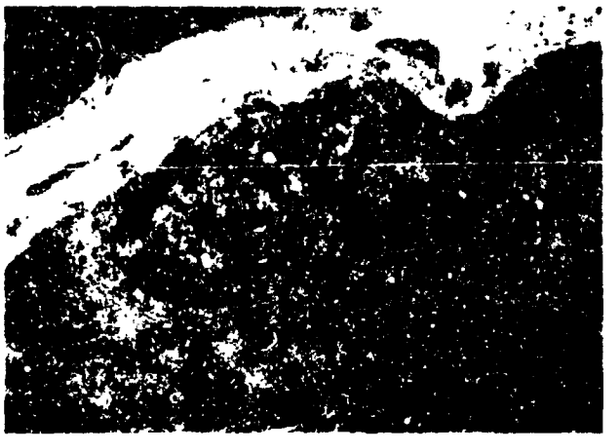

Figure 52. A quiescent satellite cell in a Flight EDL muscle. The cell has a thin rim of cytoplasm, and the nucleus is heterochromatic. X16,800.

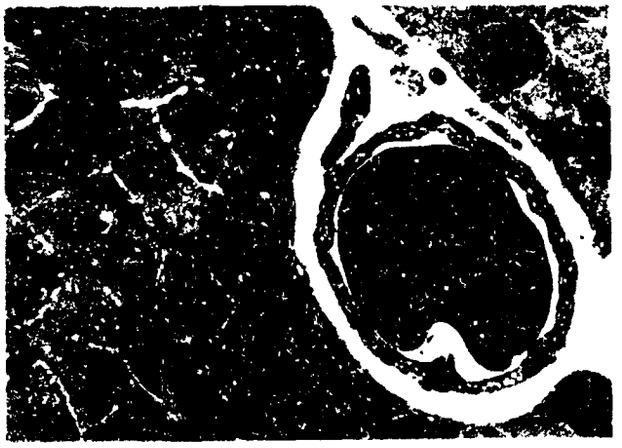

Figure 53. The capillaries in the Flight EDL muscles were not disrupted. As in control muscles, erythrocytes are often observed within the capillary lumen. X13,750.

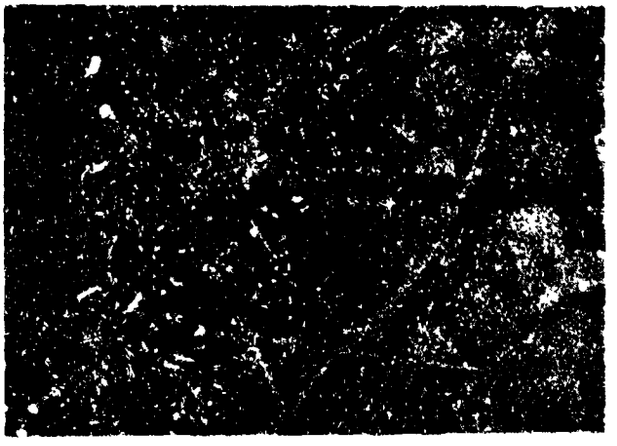

Figure 54. A cross section of an SO fiber in a Flight EDL muscle. As in normal muscles, medium-sized mitochondria surround the myofibrils at the level of the I band. X13,750.

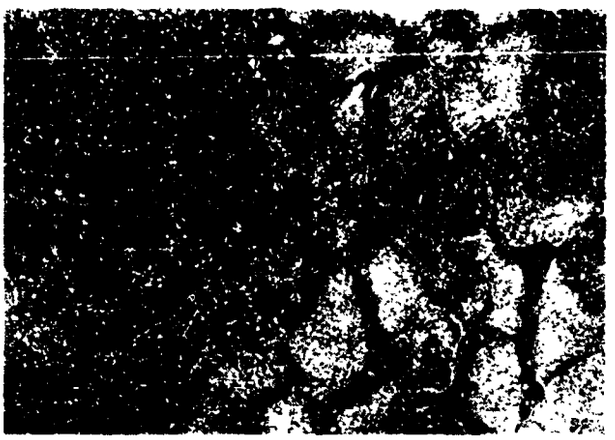

Figure 55. An FOG fiber in a Flight EDL muscle. Large mitochondria occupy the I band region and are present in the A bands. Myofibrils and membrane systems appear normal. X13,750.

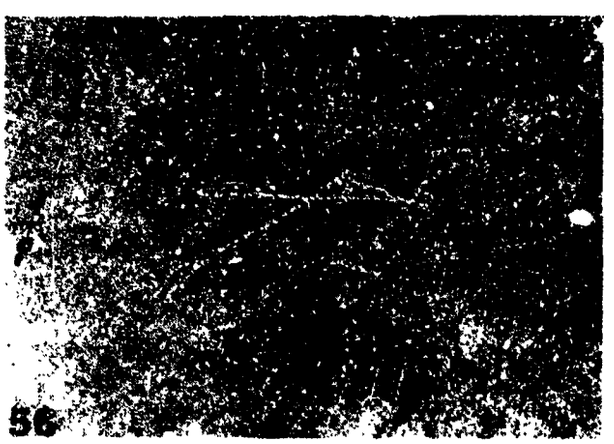

Figure 56. An FG fiber in a Flight EDL muscle. The small thin mitochondria are mostly confined to the I band region. The morphology of this fiber is indistinguishable from normal. X13,750.

EXPERIMENT K-6-09

PART II: BIOCHEMICAL ANALYSIS OF EDL AND PLT MUSCLES

S. Ellis, et al.

RESULTS

Measurements were made of two enzymes, the lysosomal tripeptidyl aminopeptidase (TAP) and the cytosolic anhydrase III (CA III), and also the calcium binding protein parvalbumin (PVA). TAP and CA III were measured as described by Riley et al (1982;1987) and PVA was measured by the electrophoretic method of Klug et al., (1983). By way of background, TAP increased 60% in the Soleus muscles after 7.5 days in the SLS-3 flight rats whereas the EDL concentrations were unchanged. Surprisingly, the PLT muscle from the Cosmos '87 rats, flown for 12.5 days, showed a 30% decrease (Table 1). The EDL did not show an increase in TAP activity.

CA III is present in highest concentrations in slow oxidative muscle fibers whereas fast fibers have very low concentrations (Riley et al., 1982), and the levels of the enzyme can be affected by a number of physiological perturbations. Although the EDL and PLT are quite gravity insensitive, it was of interest to determine the influence of space flight on the CA III levels. As can be seen from Tables I and II there was no difference in CA III content of these muscles except for the PLT of the basal group which showed a slightly slower concentration of CA III, presumably due to their younger age (90 days) (Riley et al., 1982).

Parvalbumin is highest in concentration in the fast twitch muscle and functions as a relaxing factor facilitating sequestration of calcium in the sarcoplasmic reticulum. In view of reports that unloading slows the 1/2 relaxation time, it was of interest to measure PVA for possible concentration decreases in the EDL and PLT muscles. As can be seen from Table 1, the PVA concentrations of the PLT were not significantly different in any of the groups. In the case of the EDL, only the synchronous group showed a significant reduction in PVA, whereas the basal, vivarium, and flight groups did not differ.

Thus, space flight showed significant perturbation only in the TAP concentration of the PLT, the concentrations of the CA III and the PVA being unaffected in either of the two muscles. It should be noted that these results may have been quantitatively affected by a thaw to room temperatures for approximately twenty-four hours due to a failure in the emergency back-up electrical power to our minus 80°C freezers. Simulation of the thawed condition for twenty-four hours using fresh muscles showed no reduction in TAP or CA III activities, whereas PVA was reduced by 24% in the EDL (6.8 to 5.1 µg/mg wet muscle) and unchanged in the PLT (3.9 µg/mg wet muscle), the muscles being sampled from 250g rats. These observations suggest that the thawing would not affect the conclusions or reliability to a significant degree.

REFERENCES

Riley, D.A., Ellis,S., and J. Bain. J. Histochem. Cytochem. 30: 1275 (1982).

Riley, D.A., Ellis, S., Slocum, G.R. et al. Muscle and Nerve 10: 560 (1987).

Klug, G., Reichman, H., and D. Pette. FEBS Lett. 152: 180 (1983).

TABLE 1

SUMMARY OF ASSAYS OF PLANTARIS MUSCLE

ACTIVITY

GROUP and RAT NO.	CA III U/mg muscle	TAP mU/mg Muscle	PVA ug/mg muscle
BASAL			
B_6	0.88	0.10	2.26
B_7	0.89	0.08	2.93
B_8	0.76	0.15	2.71
B_9	0.96	0.08	3.10
B_{10}	0.97	0.16	3.45
	0.89 ±.05 (B vs S: p <.05)	0.11±.038	2.89±0.44
VIVARIUM			
V_6	0.63	0.09	2.21
V_7	1.2	0.10	2.36
V_8	1.0	0.11	4.12
V_9	0.90	0.11	5.41
V_{10}	1.1	0.11	3.77
	0.97 ± .21	0.10 ± .01	3.57 ±1.32
SYNCHRONOUS			
S_6	0.97	0.10	2.05
S_7	1.0	0.11	2.96
S_8	1.1	0.12	3.14
S_9	1.0	0.14	2.58
S_{10}	0.95	---	3.14
	0.96 ±.058	0.12 ±.02	2.77 ±.47
FLIGHT			
F_6	1.1	0.11	2.74
F_7	1.04	0.07	2.68
F_8	0.64	0.08	3.53
F_9	1.1	0.09	4.14
F_{10}	0.97	0.04	4.09
	0.97 ±.19	0.078 ±.026	3.44 ±0.71
		(F vs S: p<.05)	

Note 1: CA III and PVA columns: Means of triplicate analysis per sample.
Note 2: p values from t statistic for two means.

TABLE 2

SUMMARY OF ASSAYS OF EDL MUSCLE

ACTIVITY

GROUP and RAT NO.	CA III U/mg muscle	TAP mU/mg muscle	PVA ug/mg muscle
BASAL			
B_6	0.11	0.24	---
B_7	0.14	0.11	2.80
B_8	0.10	0.28	3.53
B_9	0.19	0.28	3.90
B_{10}	0.13	0.40	5.06
	0.134 ±.035	0.26±.10 (F vs B: p <0.05)	3.82±.94
VIVARIUM			
V_6	0.13	0.13	---
V_7	0.18	0.32	4.24
V_8	0.21	0.14	4.89
V_9	0.12	0.38	4.20
V_{10}	0.02	0.14	5.58
	0.132 ± .073	0.22 ± .12	4.73 ±0.65
SYNCHRONOUS			
S_6	0.20	0.11	3.44
S_7	0.28	0.16	3.56
S_8	0.12	0.13	2.39
S_9	0.12	0.14	1.43
S_{10}	0.25	0.15	3.66
	.194 ±.073	0.14 ±.02	2.90 ±0.97 (S vs V, p <.05)
FLIGHT			
F_6	0.20	0.14	3.69
F_7	0.06	0.12	5.28
F_8	0.08	---	3.53
F_9	0.01	0.07	4.20
F_{10}	0.23	0.14	5.39
	0.136 ±.094	0.13 ±.03	4.42±0.87 (F vs S: p<.05)

Note 1: CA III and PVA columns: Means of triplicate analysis per sample.
Note 2: p values from t statistic for two means.